Development of Potent and Selective Inhibitors for Group VIA Calcium-Independent Phospholipase A_2 Guided by Molecular Dynamics and Structure-Activity Relationships

Varnavas D. Mouchlis[*],[†], **Dimitris Limnios**[‡], **Maroula G. Kokotou**[‡], **Efrosini Barbayianni**[‡], **George Kokotos**[*],[‡], **J. Andrew McCammon**[†], and **Edward A. Dennis**[*],[†]

[†]Department of Pharmacology and Department of Chemistry and Biochemistry, School of Medicine, University of California, San Diego, La Jolla, California 92093-0601, USA

[‡]Laboratory of Organic Chemistry, Department of Chemistry, National and Kapodistrian University of Athens, Panepistimiopolis, Athens 15771, Greece

Abstract

The development of inhibitors for phospholipases A_2 (PLA_2s) is important in elucidating their implication in various biological pathways. PLA_2 enzymes are an important pharmacological target implicated in various inflammatory diseases. Computational chemistry, organic synthesis and *in vitro* assays were employed to develop potent and selective inhibitors for Group VIA calcium-independent PLA_2. A set of fluoroketone inhibitors, were studied for their binding mode with two human cytosolic PLA_2 enzymes: Group IVA $cPLA_2$ and Group VIA $iPLA_2$. New compounds were synthesized and tested against three major PLA_2 enzyme. This study led to the development of four potent and selective thioether fluoroketone inhibitors as well as a thioether keto-1,2,4-oxadiazole inhibitor for GVIA $iPLA_2$, which will serve as lead compounds for future development and studies. The keto-1,2,4-oxadiazole functionality with a thioether is a novel structure and it will be used as a lead to develop inhibitors with higher potency and selectivity towards GVIA $iPLA_2$.

Graphical abstract

[*]Corresponding Authors: For Varnavas D. Mouchlis vmouchlis@ucsd.edu. Phone: +1 858 534 8903. *For George Kokotos gkokotos@chem.uoa.gr. Phone: +30 210 7274462. *For Edward A. Dennis, edennis@ucsd.edu. Phone: +1 858 534 3055.

Supporting Information

Additional figure and toppar stream files for compounds **2**, **3**, **21**, **32** and **33** (PDF).

3D movies for MD simulation on enzyme-inhibitor complexes (mpg):

> Movie 1: GVIA $iPLA_2$-**2** complex
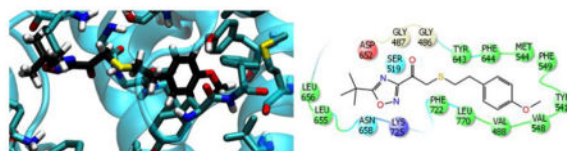>
> Movie 2: GVIA $iPLA_2$-**3** complex
>
> Movie 3: GIVA $cPLA_2$-**21** complex
>
> Movie 4: GVIA $iPLA_2$-**32** complex
>
> Movie 5: GVIA $iPLA_2$-**33** complex
>
> Data of Table 1 (CSV)
>
> Data of Table 2 (CSV)

Introduction

Phospholipase A_2 (PLA$_2$) constitutes a superfamily of enzymes that currently consists of 16 groups and several subgroups, and can be classified into the following six types: cytosolic (cPLA$_2$), secreted (sPLA$_2$), calcium-independent (iPLA$_2$), platelet-activating factor acetylhydrolase (PAF-AH) also known as lipoprotein-associated PLA$_2$ (Lp-PLA$_2$), lysosomal PLA$_2$ (LPLA$_2$), and adipose-PLA (AdPLA).[1] PLA$_2$s catalyze the release of free fatty acids including arachidonic acid (AA) which is the initial and rate limiting step for eicosanoid biosynthesis.[2] Through their catalytic activity, Group IVA cytosolic (GVIA cPLA$_2$), Group VIA calcium-independent (GVIA iPLA$_2$), and Group V secreted (GV sPLA$_2$) enzymes are implicated in many inflammatory diseases.[1] Thus, the development of potent and selective inhibitors for each of these three enzymes should lead to the development of novel pharmaceutical agents for different inflammatory conditions.[3]

GIVA cPLA$_2$ was cloned and sequenced in 1991[4–6] and its crystal structure was reported in 1999.[7] This enzyme utilizes a catalytic dyad of Ser/Asp, and it exhibits high specificity for membrane phospholipids containing AA at the *sn*-2 position. Thus, it is the main AA provider for the cyclooxygenase (COX) and lipoxygenase (LOX) pathways.[8] Therefore, this enzyme can be considered a key enzyme for mediating production of eicosanoids which are implicated in numerous inflammatory diseases.[1]

GVIA iPLA$_2$ was purified from macrophages in 1994,[9, 10] and its crystal structure has not been solved yet. The human gene of this enzyme expresses multiple splice variants.[11, 12] Among them, the transcript variant 1 is one of the two active isoforms in humans. GVIA iPLA$_2$ also utilizes a catalytic dyad of Ser/Asp, and it is not known to exhibit specificity for the *sn*-2 fatty acid of the membrane phospholipids. It was found to be involved in membrane homeostasis and remodeling involved in the basic metabolic functions within the cell.[1, 13] GVIA iPLA$_2$ is involved in signaling and other pathological conditions including diabetes[14] and Barth syndrome.[15]

GV sPLA$_2$ was expressed and characterized in 1998,[16] and its crystal structure has not been reported either. This enzyme is also implicated in several inflammatory diseases, and its activity was found to be interrelated with that of GIVA cPLA$_2$.[17] GV sPLA$_2$ utilizes a catalytic dyad of His/Asp, and it was detected in rheumatoid arthritis synovial fluids, but its expression was significantly lower than GIIA sPLA$_2$, which is the major enzyme secreted in rheumatoid arthritis.[18]

A variety of diverse small molecule inhibitors have been reported and their structures are summarized in review articles.[19, 20] Our groups have developed some novel classes of inhibitors including 2-oxoamides for GIVA cPLA$_2$,[21, 22] amides for GV sPLA$_2$,[23] and

fluoroketones for GVIA iPLA$_2$.[24–26] We have now explored potent and selective inhibitors for GVIA iPLA$_2$ using structure-based design and *in vitro* mixed micelle assays.[27] Even though there is no available crystal structure for this enzyme, we have developed a robust homology model based on hydrogen/deuterium exchange mass spectrometry (DXMS) experimental data and molecular dynamics (MD) simulations.[28–30] The 3D structure of GVIA iPLA$_2$ was used for molecular docking calculations and MD simulations with previously synthesized inhibitors in an effort to establish a structure-activity relationship (SAR). Based on our SAR model, new fluoroketone compounds were designed, synthesized and tested *in vitro*, and we were able to identify four new fluoroketones that potently inhibit GVIA iPLA$_2$ and they are quite selective relative to GIVA cPLA$_2$ and GV sPLA$_2$. In addition, a novel potent and selective GVIA iPLA$_2$ inhibitor based on a keto-1,2,4-oxadiazole functionality with a thioether was identify.

Results and Discussion

Structure-based design protocol

Fluoroketones represent a unique class of PLA$_2$ inhibitors that are highly potent and selective toward GVIA iPLA$_2$.[24–26] Understanding the binding mode (conformation of the inhibitor as well as its interactions with the binding pocket of the enzyme) of these compounds is crucial in designing new compounds with improved inhibitory properties. To do so, a data set of 27 PLA$_2$ inhibitors was used in order to develop a SAR for designing, synthesizing and testing new compounds (Table 1).[24, 25] Figure 1 schematically represents the structure-based design approach adopted in this study with the goal to design, synthesize and test new fluoroketone compounds for their inhibitory activity against representatives of three major PLA$_2$ groups.

Three compounds were initially selected and docked in the binding pocket of both GVIA iPLA$_2$ and GIVA cPLA$_2$. GV sPLA$_2$ was not included in the structure-based design protocol because none of the fluoroketone compounds exhibited significant activity towards this enzyme.[24, 25] Compounds **2** (GK187)[25] and **3** (FKGK18)[24] are potent inhibitors of GVIA iPLA$_2$ that showed similar inhibitory activity (Table 1). Compound **2** is a pentafluoro ketone containing a methoxy phenyl group, while compound **3** is a trifluoromethyl ketone with a naphthalene group at the hydrophobic chain. These two compounds were used to initiate our studies because they are structurally different in terms of the fluoro carbonyl as well as the hydrophobic chain even though they have comparable inhibitory potency.[24, 25] Compound **21** (GK174)[25] is a trifluoromethyl ketone with two phenyl groups at the hydrophobic chain and is the only compound in this class that showed high inhibitory activity against GIVA cPLA$_2$.[25] Each compound was docked in the binding pocket of the relevant enzyme to create an optimized enzyme-inhibitor complex in terms of conformation and binding energy. The resulting enzyme-inhibitor complexes were then placed on a POPC membrane patch based on previously published models,[28] and the systems (enzyme-inhibitor-membrane-water) were minimized, equilibrated and subjected to a 300 ns simulation each. Clustering analysis was performed to identify the most abundant conformation for each complex. These complexes were used in docking calculations using a set of published fluoroketone

inhibitors[24, 25] with the goal to create reliable models to assist the structure-based design of new compounds.

Binding mode of fluoroketone inhibitors based on Induced Fit Docking (IFD)

The IFD calculations were performed using the homology model of GVIA iPLA$_2$28 and the crystal structure for GIVA cPLA$_2$.[7] Residues Gly486, Gly487, Lys489, Ser519, Val548, Phe549, Leu560, Tyr643, Phe644, Asp652, Lys729, and Leu770 were selected to define the binding pocket of GVIA iPLA$_2$ in the IFD calculations. These residues were found to show decreased "on exchange" rates in DXMS studies upon binding of a GVIA iPLA$_2$ inhibitor, which belongs to the same fluoroketone class of compounds.[30] For GIVA cPLA$_2$ residues Gly197, Gly198, Phe199, Arg200, Ser228, Trp232, Pro263, Phe295, Leu298, Ile299, Thr302, Leu303, Phe397, Met417, Asp549, Asn555, Thr680 and Phe683 were chosen to define the binding pocket of the enzyme in the IFD calculations. These residues showed decreased "on exchange" rates in DXMS studies upon binding with pyrrophenone, which is a potent GIVA cPLA$_2$ inhibitor.[31]

Figure 2A and 2C show the binding mode of compound **2** and **3** in the binding pocket of GVIA iPLA$_2$ generated by the IFD calculations. The fluoroketone group is located in the hydrophilic region of the binding pocket. The oxygen atom of the carbonyl group is near to residues Gly486/Gly487 which constitute the "oxyanion hole". These two glycine residues were found to interact with the *sn*-2 carbonyl group of the phospholipid according to our previously published structural studies.[28] The same oxygen atom is in spatial proximity to the catalytic Ser519. The fluorine atoms are located near to the residues Asn658 and Lys725. These two residues were found to interact with the phosphate group according to our previous studies.[28] The methoxy phenyl group in compound **2** and the naphthalene group in **3** is located near to the entrance of the binding pocket, and it interacts with aromatic and aliphatic residues including Val548, Phe549, Leu560, Tyr643, Phe644 and Leu770 (Fig. 2A and 2C).

Figure 3A represents the binding mode of compound **21** in the binding pocket of GIVA cPLA$_2$ from the IFD calculations. The fluoroketone group is located near to the "oxyanion hole" (Gly197/Gly198) and to the catalytic Ser228, with fluorine atoms near Asn555. It seems that the binding of the fluoroketone group in both enzymes involves identical residues. These residues were also found to interact either with the *sn*-2 carbonyl group (Gly197/Gly198) or the phosphate group (Asn555) of the phospholipid molecule in our previous studies.[28] The two phenyl groups are placed in the hydrophobic region of the active site near residues Trp232, Pro263, Phe295, Leu298, Ile299, Thr302, Leu303, Phe397 and Phe683. This is the region where the fatty acyl chains of the phospholipid molecule were bound according to our previous studies.[28]

Binding mode of fluoroketone inhibitors after MD

Each enzyme-inhibitor complex was placed on the surface of a POPC membrane patch (Fig. 1) minimized, equilibrated and subjected to a 300 ns simulation using NAMD 2.9.[32] The RMSD for the enzyme backbone atoms was stabilized at ~2.5 Å relative to the starting structure indicating that each simulation was reasonably converged (Fig. S1).

The binding mode of compound **2** and **3** after the MD simulation is shown in Figure 2B and 2D. The fluoroketone group remains in the hydrophilic region of the enzyme binding pocket with the oxygen atom of each carbonyl group interacting periodically with Gly486/Gly487 the so called "oxyanion hole" (Movie 1 and 2 or Fig. 2B and 2D). The same oxygen atom does not show any interactions with the catalytic Ser519. The fluorine atoms participate in H-bonding interactions with residue Asn658 but no interactions were observed with residue Lys725. In both simulations, the fluoroketone group shows an identical interaction pattern while the number of fluorine atoms does not seem to play a significant role in the binding. The simulations showed an interesting movement of the methoxy phenyl group in **2** and the naphthalene group in **3** from the entrance of the active site into the hydrophobic region of the binding pocket (Movie 1 and 2). The final pose of the MD simulations shows the two compounds in a horizontal orientation (Fig. 2B and 2D) rather than the vertical one suggested by the IFD complexes (Fig. 2A and 2C). This hydrophobic region was found to accommodate the *sn*-2 fatty acyl chain during our previously published studies on a PAPC substrate.[28] On their final binding mode, the two groups were found to interact with residues like Val488, Ile523, Tyr541, Met544, Val548, Phe549, Leu560, Tyr643, Phe644 and Leu770. It is worth mentioning that the oxygen atom of the methoxy phenyl group participates in H-bonding with Tyr541 during the simulation (Movie 1).

The MD simulation of the GIVA cPLA$_2$–**21** complex (Fig. 3B) shows that the oxygen atom of the fluoroketone carbonyl group interacts with Gly197/Gly198, the so called "oxyanion hole" (Movie 3 or Fig. 3B). The fluorine atoms are in spatial proximity with Asn555 but no H-bonding interactions were observed during the simulation. The distance between the nitrogen atom of Asn555 and the fluorine atoms ranges between 3.0 to 3.5 Å, but never drops below 2.8 which is the threshold for the formation of an H-bond. The two phenyl groups remain in the same hydrophobic region of the deep binding channel indicated by the IFD complex and they do not appear to change their binding mode significantly during the simulation (Movie 3 or Fig. 3B).

Structure-activity relationships (SAR)

A representative enzyme-inhibitor complex was selected from each of the five clusters (Fig. 1) for docking calculations. Each complex was optimized using the Protein Preparation Wizard (PPW),[33] and the already bound inhibitor was redocked in the active site. Enzyme-inhibitor complexes that belong to the most abundant clusters received the highest (absolute value) theoretical binding score, named herein as the XP GScore (Extra-Precision Glide Score). Compound **2** and **3** received similar XP GScore towards each MD complex with **3** showing slightly more optimized H-Bonding interactions. Thus, 3D complex of GVIA iPLA$_2$ with compound **3** was used for conducting docking calculations for the SAR studies. All the fluoroketone compounds of Table 1[24, 25] were docked in GVIA iPLA2 binding site in order to examine if the structural models can give a good correlation between inhibitory activity and XP GScore. Table 1 summarizes the structures, the $X_I(50)$, the log $X_I(50)$, and the XP GScore for the selected compounds. $X_I(50)$ is the mole fraction of the compound that is required for 50% inhibition of the enzyme. Mole fraction is a dimensionless number derived by dividing the number of moles of inhibitor by the total number of moles of surface (moles of substrate plus inhibitor plus detergent).[34, 35] $X_I(50)$ values can be converted to

molar concentration by considering that 0.091 mole faction of inhibitor corresponds to 50 μM concentration. Thus, an $X_I(50)$ of 0.0001 corresponds to 55 nM.

An initial linear regression analysis did not reveal a correlation between the $X_I(50)$ and XP GScore values (Fig. 4A, Table 1). However, further analysis of the results showed that compounds **6**, **8** and **12** give false negative predictions, while compounds **22** and **24** give false positive predictions according to the XP Glide scoring function. Outliers are typical of docking calculations since empirical scoring functions are not completely accurate in calculating theoretical binding scores.[36] By excluding these five compounds from the linear regression, the linearity was significantly improved (Fig. 4B). It is worth noting that the compounds with high $X_I(50)$ values tend to have higher XP GScore against GVIA iPLA$_2$, with our lead compounds **2** and **3** ranked among the highest ones. Another interesting compound is **21** which is the only compound exhibiting significant inhibitory activity against GIVA cPLA$_2$ ($X_I(50) = 0.0074$). This compound ranked with the highest XP GScore against GIVA cPLA$_2$ in comparison with the lower scored **2** and **3** which showed no significant activity against GIVA cPLA$_2$ (Table 1).

Design and synthesis of thioether fluoroketone and keto-1,2,4-oxadiazole inhibitors using the SAR model

In order to test the predictive ability of our SAR models, we have designed four new fluoroketone compounds based on the structures of compound **1** (GK177),[25] **2**, **3** and **10** (FKGK11, Table 1).[24, 25] These new analogues (**28**, **29**, **30**, and **31** in Table 2) contain a sulfur atom at the beta position to the carbonyl group taking into consideration the following literature data. During the '80s, Hammock and coworkers demonstrated that in some cases the presence of a thioether beta to the carbonyl group of trifluoromethyl ketones increased the inhibitory potency on juvenile hormone esterase[37] and mammalian carboxylesterase.[38] In addition, polyunsaturated trifluoromethyl ketones containing sulfur or oxygen atoms at the beta position were synthesized starting from EPA and DHA as potential PLA$_2$ inhibitors.[39] Recently, it was demonstrated that such sulfur derivatives directly inhibit GIVA cPLA$_2$ and suppress PGE$_2$ formation in mesangial cells.[40] Given the substantial structural similarity of the new compounds with their original analogues we also synthesized two novel compounds (**32** and **33** in Table 2) containing a 1,2,4-oxadiazole ring in order to test the ability of the SAR model to predict structurally different compounds. Oxadiazoles compounds were developed in the past as inhibitors of various enzymes including HIV integrase and they have been proven to exhibit a wide range of biological activities.[41, 42]

Two different routes were employed to synthesize fluoroketones containing a sulfur atom at the beta position to activated carbonyl. Thiols **34a–c** were reacted with commercially available 3-bromo-1,1,1-trifluoroacetone or 1-bromo-3,3,4,4,4-pentafluorobutan-2-one to give directly the target compounds **28, 30, 31** (Scheme 1). Pentafluoro derivative **29** was prepared by conversion of carboxylic acid **35** to the corresponding Weinreb amide, followed by treatment with (pentafluoroethyl)lithium (Scheme 1). Both routes led to products in high yield and in conclusion the synthesis of these new thioether fluoroketones requires fewer steps in comparison to the synthesis of compound **1**, **2** and **3**, where the synthesis starts from

the Horner-Emmons reaction of an appropriate aromatic aldehyde and triethyl phosphonocrotonate.

The synthesis of keto-1,2,4-oxadiazoles is depicted in Scheme 2. Alcohols **36a,b** were oxidized to aldehydes and treated with *tert*-butyldimethylsilyl cyanide (TBDMSCN) in the presence of KCN and 18-crown-6 to produce nitriles **37a,b**. Then, amidoximes **38a,b** were prepared and coupled with pivalic acid using *N,N'*-dicyclocarbodiimide (DCC) as the coupling agent to give compounds **39a,b**. The formation of the 1,2,4-oxadiazole ring was accomplished by treatment with tetrabutylammonium fluoride (TBAF) under microwave irradiation. Under such conditions the silyl protecting group was removed and compounds **40a,b** were finally oxidized to target compounds **32, 33** using the Dess-Martin reagent.

As shown in Table 2, our SAR model ranked compounds **28** (GK407), **29** (GK388) and **30** (GK408) with an XP GScore as high as the ones for **1**, **2** and **3** against GVIA iPLA$_2$, and as low as the ones against GIVA cPLA$_2$. These compounds were tested *in vitro* against GVIA iPLA$_2$ and GIVA cPLA$_2$ and they indeed showed a comparable inhibitory activity and selectivity against GVIA iPLA$_2$ as their precursor compounds. They also showed negligible inhibitory activity against the GV sPLA$_2$, as expected for this class of fluoroketones. It is worth mentioning that compound **3** and **30** gave a higher XP GScore against GIVA cPLA$_2$ than **1**, **2**, **28** and **29** and they also showed a higher percentage of inhibition against GIVA cPLA$_2$ (inhibition 80.8% against GIVA cPLA$_2$ was reported for compound **3**).[24] The importance of the sulfur atom for the potency of these inhibitors indicated by dramatic improvement of the inhibitory activity of compound **31** (Table 2) which is 10-fold more potent than its non-thio analogue **10** (Table 1). This compound shows high potency and selectivity for GVIA iPLA$_2$ and it was ranked among the highly active compounds by receiving an XP GScore of 8.4. Finally, the potency of compounds **32** (GK392) and **33** (GK367) towards GVIA iPLA$_2$ was satisfactorily predicted by the SAR model even though the compounds are structurally different from fluoroketones. Compound **32** received an XP score of 7.4 and an $X_I(50)$ of 0.0057 in contrast with it non-thio analogue **33** which received and XP of 4.8 and insignificant inhibition towards GVIA iPLA$_2$. The selectivity of **32** towards GVIA iPLA$_2$ was also predicted by receiving low XP GScore towards GIVA cPLA$_2$.

Understanding the binding of the fluoroketone group

Our structural model gives insight into the binding mode of fluoroketone inhibitors as potent and selective inhibitors of GVIA iPLA$_2$. Starting with the fluoroketone group it is clear that the number of fluorine atoms does not play a central role in the inhibitory activity. Both trifluoromethyl and pentafluoroethyl ketone gave the same activity (**1** and **2** in Table 1).[25] Simulations of both compounds **2** and **3** showed one residue Asn658 in GVIA iPLA$_2$ interacting with the fluorine atoms of both pentafluoroethyl and trifluoromethyl groups (Movie 1 and 2). According to our proposed catalytic cycle, the "oxyanion hole" stabilizes the tetrahedral intermediate formed after the Ser519 attacks the carbon atom of the *sn*-2 carbonyl group.[28] It is likely that the fluorine atoms add to the polarity of the carbonyl group and the catalytic Ser519 attacks the carbon atom forming a reversible hemiacetal, while residues Gly486/Gly487 stabilize the negatively charged oxygen atom. Based on our

mechanistic assumptions, it appears that our model works well. However, the possibility of the formation of a covalent bond cannot be excluded, but that would not change the conclusion significantly. It is worth mentioning that the interactions of the fluoroketone group in GIVA cPLA$_2$ (Movie 3) are identical with the ones in GVIA iPLA$_2$.

Understanding the binding of the hydrophobic chain

The hydrophobic chain appears to play a critical role in the inhibitory activity of these compounds. The aromatic rings participate in pi-pi stacking while the bulky naphthalene ring in compound **3** reduces the inhibitory activity two-fold in contrast to the methoxy phenyl group in **2**. The simulations (Movie 1 and 2) show that the methoxy phenyl group is much more flexible during its accommodation in the hydrophobic region of the pocket and, thus, optimizes its interactions with the surrounding residues. Moreover, the oxygen atom forms an H-bond with residue Tyr541 making the binding of **2** more favorable (Movie 1). The hydrophobic chain also plays an important role in the selectivity of these compounds. Short compounds like **2** show high selectivity toward GVIA iPLA$_2$, while they tend to lose selectivity when the chain becomes bulkier (compound **3** exhibits less selectivity) and longer (compound **21** shows no selectivity). Our studies on the binding of a PAPC molecule,[28] indicated that GIVA cPLA$_2$ has a much deeper channel-like binding pocket than GVIA iPLA$_2$. As a result, fluoroketones with a long hydrophobic chain will complement better the deep pocket and they will have higher inhibitory potency.

In summary, our studies show that the same fluoroketone functional group (activated carbonyl group) can be used to develop inhibitors with selectivity for either GVIA iPLA$_2$ or GIVA cPLA$_2$, which share the same catalytic mechanism both utilizing a catalytic dyad of Ser/Asp. However, the size of the hydrophobic chain is very critical for both activity and selectivity. Short-chain compounds tend to prefer GVIA iPLA$_2$ while long-chain compounds also inhibit GIVA cPLA$_2$.

Thioether enhances inhibitor binding and potency

MD simulations on compounds **32** and **33** revealed the binding mode of these two compounds and how the sulfur atom improves the inhibitory potency of the thio-analogues. The binding mode of **32** that occur during the simulation (Fig. 5A) showed that this compound exhibits tighter binding than **33** (Fig. 5B). It is obvious that the phenyl ring of **32** is closer to the residues of the hydrophobic pocket of GVIA iPLA$_2$. The MD simulations showed that **32** (Movie 4) is much more stable in the binding site of the enzyme in comparison with **33** (Movie 5). The carbonyl group is constantly interacting with the "oxyanion hole" (Gly486/Gly487) while theoxadiazole ring is forming H-Bonds with Asn658. The same interactions do not occur in the case of **33** making its binding weaker and as a results is very unstable in the binding site of the enzyme during the simulation (Movie 5). The sulfur atom is also a very versatile atom in terms of its interactions with the residues of an enzyme. Its electron cloud can be involved in pi-pi stacking interactions and other interaction with aromatic or non-aromatic residues.[43] In the case of **32** the sulfur atom is in spatial proximity to Tyr643, Phe722, Leu770 as well as the "oxyanion hole" (Gly486/Gly487) constantly interacting with this residues (Movie 4). According to the X$_I$(50) value of the thio versus non-thio inhibitors, it is obvious that the presence of the beta-thioether

enhances the binding and potency of these compounds and the MD simulations clearly explain the beneficial effect of the sulfur atom upon binding of **32** (Fig. 5A and Movie 4).

Conclusion

Fluoroketones exhibit unique inhibitory properties against PLA_2 enzymes that belong to serine hydrolases and, thus, are attractive synthetic compounds for elucidating the binding mode with each particular enzyme and performing structure-activity relationship studies. Our computational studies allow us to understand clearly how fluoroketones interact with either GVIA $iPLA_2$ or GIVA $cPLA_2$, and what structural features an inhibitor should possess in order to present selectivity for GVIA $iPLA_2$ or GIVA $cPLA_2$. These studies constitute a valuable guide indicating that inhibitors of GVIA $iPLA_2$ should be small-size molecules. Increase of the size and the lipophilicity of the inhibitor lead to decrease of selectivity for GVIA $iPLA_2$. An SAR model was established and new compounds were synthesized and tested that show high inhibitory activity against GVIA $iPLA_2$ while showing the validity of our structural and SAR models. In conclusion, this study introduces a new class of thioether fluoroketones that have the potential for further development in order to identify potent and selective inhibitors not only for GVIA $iPLA_2$ but for GIVA $cPLA_2$ as well. In addition, a novel structure of GVIA $iPLA_2$ inhibitor combining the keto-1,2,4-oxadiazole functionality with a thioether was identify.

Experimental Procedures

Induced Fit Docking (IFD) protocol

Each enzyme-inhibitor initial complexes were predicted using the IFD protocol implemented in Schrödinger Suite 2014.[44, 45] The enzyme 3D structure (receptor) was optimized using the PPW module.[33] The inhibitor 3D structures (ligand) were sketched using Maestro 9.9 sketcher,[46] and they were optimized using the LigPrep 3.2 application.[47] IFD protocol employs Glide 6.5[48] and the refinement module in Prime 3.8[49] to accurately predict enzyme-inhibitor complexes by incorporating side-chain flexibility for the receptor. The box center for the docking calculations was defined using the centroid of selected residues that were found to constitute the binding pocket of GVIA $iPLA_2$ and GIVA $cPLA_2$ using DXMS and extensive MD simulations in our previously published papers.[28–30] The box size was determined automatically according to the centroid of the specified binding pocket residues. For the initial docking of the inhibitors the side-chain of the binding pocket residues were trimmed automatically based on the B-factor. The receptor van der Waals scaling was set to 0.70 and the ligand van der Waals scaling to 0.50. Twenty poses (binding modes) of each inhibitor were allowed to pass to the Prime refinement step. During the Prime refinement step, the side-chains of the residues within 6 Å the inhibitor pose were optimized in terms of conformation and potential energy. Finally, twenty enzyme-inhibitor structures were allowed to pass to the redocking step with a threshold for eliminating high-energy structures from the Prime refinement of 30 kcal/mol, and the Glide Extra-Precision (XP) scoring function.[50] The final complexes were selected based on the binding mode and the score.

Molecular Dynamics (MD) simulations

MD simulations were carried out on enzyme-inhibitor complexes (compounds **2**, **3**, **32** and **33** for GVIA iPLA$_2$, and compound **21** for GIVA cPLA$_2$), which were derived from the docking calculations. Each complex was placed on a POPC membrane patch of ~100 × 100 Å^2 area according to our previously published model.[28–30] POPC molecules within 0.6 Å of the enzyme were removed, the system was solvated with TIP3P water molecules, and was neutralized using sodium chloride at a concentration of 100 mM. The total number of atoms of the entire system was approximately 105,000. NAMD 2.9 was employed for the MD simulations.[32] The CHARMM General Force Field (CGenFF) and parameters were used for the inhibitors,[51] and the CHARMM36 all-atom additive force field and parameters were used for the enzyme and the POPC membrane patch.[52] The system was minimized for 20,000 steps and equilibrated for 12 ns to relieve all the unfavorable contacts. Finally, a 300 ns MD simulation was performed at a temperature of 310 K using the *NPT* ensemble. The trajectory files of the simulations were analyzed using the Visual Molecular Dynamics (VMD) software.[53]

Docking Calculations

Clustering analysis was performed on the trajectories derived from the MD simulations on the enzyme-**2**, -**3** and -**21** complexes in order to identify suitable conformations for the docking calculations. The 3D structures were optimized using the PPW.[33] The 3D structures of the inhibitors were sketched using Maestro 9.9 sketcher[46] and they were optimized using LigPrep 3.2.[47] Glide 5.8 was used for the rigid-docking of the compounds into the enzyme binding pocket.[48] The grid required for the docking procedure was generated using a scaling factor of 1.0 and partial charge cutoff of 0.25, while *X*, *Y*, *Z* dimensions of the inner box were set to 12 Å. For the inhibitor docking a scaling factor of 0.8 and partial charge cutoff of 0.15 were used that allow complete flexibility of the structures. The poses were selected according to the binding mode and the XP GScore. The Glide Extra-Precision (XP) scoring function[50] was used for the calculations.

In vitro PLA$_2$ activity Assay

The activities of human GVIA iPLA$_2$, GIV cPLA$_2$ and GV sPLA$_2$ were determine using a group-specific mixed micelle modified Dole assay.[21, 27] The substrate was prepared using slightly different conditions for each enzyme to achieve optimum activity: (i) GVIA iPLA$_2$ mixed micelle substrate consisted of 400 μM Triton X-100, 98.3 μM PAPC, and 1.7μM arachidonyl-1–[14]C PAPC in a buffer containing 100 mM HEPES pH 7.5, 2 mM ATP, and 4 mM DTT; (ii) GIVA cPLA$_2$ mixed micelle substrate consisted of 400 μM Triton X-100, 95.3 μM PAPC, 1.7 μM arachidonyl-1–[14]C PAPC, and 3 μM PI(4,5)P2 in a buffer containing 100 mM HEPES pH 7.5, 90 μM CaCl$_2$, 2 mM DTT, and 0.1 mg/ml BSA; and (iii) GV sPLA$_2$ mixed micelles substrate consisted of 400 μM Triton X-100, 98.3 μM PAPC, and 1.7 μM arachidonyl-1–[14]C PAPC in a buffer containing 50 mM Tris-HCl pH 8.0, and 5 mM CaCl$_2$. The compounds were initially screened at 0.091 mole fraction (5 μL of 5 mM inhibitor in DMSO) in substrate (495 uL). X$_I$(50) was determined for compounds exhibiting greater than 95% inhibition. Inhibition curves were generated using GraphPad Prism 5.0 and the non-

linear regression by plotting percentage of inhibition vs log (mole fraction) to calculate the reported $X_I(50)$ and its associated error.

Synthesis of the inhibitors. General Methods

Chromatographic purification of products was accomplished using Merck Silica Gel 60 (70–230 or 230–400 mesh). Thin-layer chromatography (TLC) was performed on Silica Gel 60 F254 aluminum plates. Spots were visualized with UV light and/or phosphomolybdic acid in EtOH. Melting points were determined using a Bu chi 530 apparatus and were uncorrected. ^{1}H, ^{13}C and ^{19}F NMR spectra were recorded on a Varian Mercury. Chemical shifts are given in ppm, and coupling constants (J), in Hz. Peak multiplicities are described as follows: s, singlet; d, doublet; t, triplet; and m, multiplet. HRMS spectra were recorded on a Bruker Maxis Impact QTOF Spectrometer. Dichloromethane was dried by standard procedures and stored over molecular sieves. All other solvents and chemicals were reagent grade and used without further purification. The purity of all compounds subjected to biological tests was determined by analytical HPLC and was found to be 95%.

Synthesis of Fluoroketones 28, 30, 31

Thiol **34a-c** (1 mmol) was transferred to an oven dried flask and CCl_4 (2 mL) was added under nitrogen atmosphere. After 5 minutes, 3-bromo-1,1,1-trifluoropropan-2-one (1.3 mmol, 248 mg) or 1-bromo-3,3,4,4,4-pentafluorobutan-2-one (1.3 mmol, 313 mg) was added dropwise over 15 minutes. The mixture was left stirring under nitrogen bubling at room temperature for 4 hours. Column chromatography of the crude mixture afforded the desired product [EtOAc/petroleum ether (bp 40–60 °C)].

1,1,1-Trifluoro-3-((4-methoxyphenethyl)thio)propan-2-one (in equilibrium with its corresponding *gem*-diol) (28)

Yield 88%; colourless oil; ^{1}H NMR (200 MHz, $CDCl_3$) : δ 7.16–7.09 (2H, m, ArH), 6.90–6.82 (2H, m, ArH), 4.09 [1H, br s, SCH_2C(OH)$_2$], 3.80 (3H, s, OMe), 3.47 (1H, br s, SCH$_2$C=O), 3.01–2.70 (4.5H, m, 4 x CHH and 0.5 x OH), 1.81 (0.5H, br, OH); ^{13}C NMR (50 MHz, $CDCl_3$) : δ 185.1 (q, J = 34 Hz, C=O), 158.2, 131.7, 129.5, 122.8 (q, J = 285 Hz, CF$_3$), 114.3, 92.4 [q, J = 32 Hz, C(OH)$_2$], 55.2, 36.3, 35.0, 34.8, 34.7, 34.3, 33.5; ^{19}F NMR (186 MHz, $CDCl_3$) : δ -20.8, -30.3; HRMS (ESI) calcd for $C_{12}H_{12}F_3O_2S$ [M-H] $^-$, 277.0516; found, 277.0515.

1,1,1-Trifluoro-3-((2-(naphthalen-2-yl)ethyl)thio)propan-2-one (in equilibrium with its corresponding *gem*-diol) (30)

Yield 83%; colourless oil; ^{1}H NMR (200 MHz, $CDCl_3$) : δ 7.89–7.77 (3H, m, ArH), 7.67 (1H, s, ArH), 7.54–7.44 (2H, m, ArH), 7.39–7.30 (1H, m, ArH), 4.14 [1.8H, br s, SCH_2C(OH)$_2$], 3.49 (0.2H, SCH$_2$C=O), 3.12–2.90 (4H, m, 4 x CHH), 2.98 (1.8H, br, OH); ^{13}C NMR (50 MHz, $CDCl_3$) : δ 137.1, 133.5, 133.4, 128.2, 127.7, 127.5, 126.9, 126.4, 126.2, 125.6, 123.0 (q, J = 282.5 Hz, CF$_3$), 92.5 [q, J = 29 Hz, C(OH)$_2$], 36.4, 35.8, 35.1, 34.6, 34.2, 33.4; ^{19}F NMR (186 MHz, $CDCl_3$) : δ −20.7, −30.2; HRMS (ESI) calcd for $C_{15}H_{12}F_3OS$ [M-H]$^-$, 297.0566; found, 297.0563.

3,3,4,4,4-Pentafluoro-1-(phenethylthio)butan-2-one (in equilibrium with its corresponding *gem*-diol) (31)

Yield 78%; colourless oil; ^{1}H NMR (200 MHz, CDCl$_3$) : δ 7.40–7.12 (5H, m, ArH), 3.73 (0.2H, br s, OH), 3.50 (3H, s, OMe, SCH$_2$), 3.28 (0.2H, br s, OH), 3.10–2.60 (4H, m, 4 x C*H*H); ^{13}C NMR (50 MHz, CDCl$_3$) : δ 187.5 (t, J = 26.1 Hz, C=O), 139.6, 139.4, 128.6, 128.5, 126.7, 117.7 (qt, J = 287.1 and 34.0 Hz, CF$_3$), 107.0 (tq, 268.4 and 38.3 Hz, CF$_2$), 93.9 [m, C(OH)$_2$], 35.7, 35.4, 35.2, 34.9, 33.1, 31.9; ^{19}F NMR (186 MHz, CDCl$_3$) : δ −24.1, −26.7, −66.5, −71.6; HRMS (ESI) calcd for C$_{12}$H$_{12}$F$_3$O$_2$S [M-H] $^-$, 297.0378; found, 297.0381.

3,3,4,4,4-Pentafluoro-1-((4-methoxyphenethyl)thio)butan-2-one (29)

To a solution of 2-((4-methoxyphenethyl)thio)acetic acid (**3**) (0.9 mmol, 203 mg) in dry dichloromethane (7 mL) DMAP (1.1 mmol, 140 mg), *N,O*-dimethylhydroxylamine hydrochloride (0.9 mmol, 90 mg), *N*-methylmorpholine (0.9 mmol, 270 mg, 0.25 mL) and WSCI (0.9 mmol, 143 mg) were added consecutively. The mixture was left stirring for 24 hours at room temperature. Then, water was added (7 mL) and the aqueous phase was extracted with dichloromethane (2 x 10 mL). The combined organic phases were washed with H$_2$O, HCl 1N, H$_2$O, 4% NaOH, H$_2$O, brine (1 x 10 mL each) and dried over Na$_2$SO$_4$. Evaporation of the solvent afforded the corresponding Weinreb amide without further purification (78% yield, 0.70 mmol, 189 mg). In a round bottom flask containing the Weinreb amide under nitrogen atmosphere, dry Et$_2$O (15 mL) was added. Then, the mixture was cooled down to −78 °C and CF$_3$CF$_2$I (3.5 mmol, 858 mg) and MeLi.LiBr (2.2M in Et$_2$O, 3.5 mmol, 1.6 mL) were added consecutively. The mixture was left stirring at −78 °C for 2 hours and then for 1 hour at room temperature. Then, water (4 mL) and 10% KHSO$_4$ until pH 4–5 were added. The aqueous phase was extracted with Et$_2$O (3 x 10 mL) and the solvent was evaporated under reduced pressure. The residue was purified by flash column chromatography [EtOAc/petroleum ether (bp 40–60 °C), 1:9]. Yield 70% over two steps; colourless oil; ^{1}H NMR (200 MHz, CDCl$_3$) : δ 7.14 (2H, d, J = 8.7 Hz, ArH), 6.87 (2H, d, J = 8.7 Hz, ArH), 3.81 (3H, s, OMe), 3.51 (2H, s, CH$_2$C=O), 2.90–2.68 (4H, m, 4 x C*H*H); ^{13}C NMR (50 MHz, CDCl$_3$) : δ 187.5 (t, J = 26.0 Hz, C=O), 158.3, 131.4, 129.5, 117.7 (qt, J = 287.0 Hz and 34.0 Hz, CF$_3$), 113.9, 107.0 (tq, J = 268.4 Hz and 38.6 Hz, CF$_2$), 55.2, 35.4, 34.3, 33.4; ^{19}F NMR (186 MHz, CDCl$_3$) : δ −26.8, −65.6; HRMS (ESI) calcd for C$_{13}$H$_{12}$F$_5$O$_2$S [M-H] $^-$, 327.0484; found, 327.0482.

Synthesis of nitriles 37a,b

To a stirred solution of alcohol **36a,b** (1 mmol) in dry CH$_2$Cl$_2$ (10 mL), Dess-Martin periodinane was added (1.2 mmol, 509 mg) and the mixture was stirred for 1 h at room temperature. The organic solvent was evaporated under reduced pressure and Et$_2$O (30 mL) was added. The organic phase was washed with saturated aqueous NaHCO$_3$ (20 mL) containing Na$_2$S$_2$O$_3$ (1.5 g, 9.5 mmol), H$_2$O (20 mL), dried over Na$_2$SO$_4$, and the organic solvent was evaporated under reduced pressure.

To a stirred mixture of *tert*-butyldimethylsilyl cyanide (TBDMSCN) (1.0 mmol, 141 mg), potassium cyanide (0.2 mmol, 13 mg), and 18-crown-6 (0.4 mmol, 106 mg) in CH$_2$Cl$_2$ (15 mL) at 0 °C, a solution of the aldehyde (1.0 mmol) derived from alcohol **36a,b**, was added

dropwise over 30 min. After addition was completed, the mixture was stirred overnight at room temperature. The organic solvent was evaporated under reduced pressure and the residue was purified by column chromatography [EtOAc-petroleum ether (bp 40–60 °C), 0.5:9.5].

2-(*tert*-Butyldimethylsilyloxy)-6-(4-methoxyphenyl)hexanonitrile (37a)

Yield 76%; colourless oil; ^{1}H NMR (200 MHz, CDCl$_3$): δ 7.12 (2H, d, J = 10.0 Hz), 6.87 (2H, d, J = 8.0 Hz), 4.43 (1H, t, J = 6.0 Hz), 3.80 (3H, s), 2.62 (2H, t, J = 8.0 Hz), 1.89- 1.75 (2H, m), 1.71–1.48 (4H, m), 0.98 (9H, s), 0.25 (3H, s), 0.16 (3H, s); ^{13}C NMR (50 MHz, CDCl$_3$): δ 157.4, 133.6, 128.9, 119.7) 113.4) 61.4, 54.7, 35.8, 34.4, 30.7, 25.2, 23.7, 17.7, −5.5, −5.7; MS (ESI) m/z (%): 351.2 [(M+NH$_4$)$^+$, 100].

2-(*tert*-Butyldimethylsilyloxy)-3-(4-methoxyphenethylthio)propanenitrile (37b)

Yield 74%; colourless oil; ^{1}H NMR (200 MHz, CDCl$_3$): δ 7.10 (2H, d, J = 8.6 Hz), 6.82 (2H, d, J = 8.6 Hz), 4.91–4.60 (2H, m), 4.53–4.32 (1H, m), 3.77 (3H, s), 2.80–2.62 (4H, m), 0.94 (9H, s), 0.17 (3H, s), 0.11 (3H, s); ^{13}C NMR (50 MHz, CDCl$_3$): δ 157.9, 132.8, 129.5, 119.8, 113.8, 61.7, 55.1, 38.9, 35.2, 34.6, 25.6, 18.0, −5.2, −5.1; MS (ESI) m/z (%): 369.2 [(M+NH$_4$)$^+$, 100].

Synthesis of amidoximes 38a,b

Compound **37a,b** (1 mmol) was placed in a microwave vessel and a 50% aqueous solution of NH$_2$OH (4.0 mmol, 0.5 mL) was added. The reaction mixture was left stirring under microwave irradiation (initial setting at 50W) for 30 minutes at 120 °C. Then, water was added (10.0 mL) and the mixture was extracted with ether (2 x 10 mL). The combined extracts were washed with brine, dried over Na$_2$SO$_4$ and concentrated under reduced pressure. The product was purified by column chromatography [EtOAc-petroleum ether (bp 40–60 °C), 2:8].

(*Z*)-2-(*tert*-Butyldimethylsilyloxy)-*N'*-hydroxy-6-(4-methoxyphenyl)hexanimidamide (38a)

Yield 76%; colourless oil; ^{1}H NMR (200 MHz, CDCl$_3$): δ 7.13 (2H, d, J = 8.0 Hz), 6.86 (2H, d, J = 8.0 Hz), 4.85 (2H, s), 4.20 (1H, t, J = 6.0 Hz), 3.81 (3H, s), 2.60 (2H, t, J = 6.0 Hz), 1.85–1.61 (4H, m), 1.54–1.34 (2H, m), 0.94 (9H, s), 0.14 (6H, s); ^{13}C NMR (50 MHz, CDCl$_3$): δ 157.3, 155.5, 134.4, 129.0, 113.4, 70.7, 54.8, 36.5, 34.7, 31.2, 25.5, 24.6, 17.8, −5.2, −5.3; MS (ESI) m/z (%): 367.6 [(M+H)$^+$, 100].

(*Z*)-2-(*tert*-Butyldimethylsilyloxy)-*N'*-hydroxy-3-(4-methoxyphenethylthio)propanimidamide (38b)

Yield 64%; colourless oil; ^{1}H NMR (200 MHz, CDCl$_3$): δ 7.11 (2H, d, J = 8.6 Hz), 6.83 (2H, d, J = 8.6 Hz), 4.89–4.62 (2H, m), 4.33–4.18 (1H, m), 3.78 (3H, s), 2.89–2.65 (6H, m), 0.90 (9H, s), 0.13 (3H, s), 0.09 (3H, s); ^{13}C NMR (50 MHz, CDCl$_3$): δ 158.0, 154.8, 132.5, 129.4, 113.8, 70.8, 55.2, 39.1, 35.3, 34.6, 25.7, 18.1, −5.0, −5.1; MS (ESI) m/z (%): 385.2 [(M+H)$^+$, 100].

Synthesis of 39a,b

To a stirred solution of amidoxime **38a,b** (1.0 mmol) in dry CH_2Cl_2 (20 mL), pivalic acid (1 mmol, 102 mg) and DCC (1.1 mmol, 227 mg) were added. The reaction mixture was stirred overnight at room temperature. The organic solvent was evaporated under reduced pressure and the residue was purified by column chromatography [EtOAc-petroleum ether (bp 40–60 °C), 2:8].

(*Z*)-2-((*tert*-Butyldimethylsilyloxy)-*N'*-(pivaloyloxy)-6-(4-methoxyphenyl)hexanimidamide (39a)

Yield 76%; colourless oil; ^{1}H NMR (200 MHz, $CDCl_3$): δ 7.07 (2H, d, J = 8.0 Hz), 6.80 (2H, d, J = 8.0 Hz), 4.87 (2H, s, NH_2), 4.32 (1H, t, J = 6.0 Hz), 3.77 (3H, s), 2.54 (2H, t, J = 8.0 Hz), 1.83–1.60 (6H, m), 1.28 (9H, s), 0.88 (9H, s), 0.07 (6H, s); ^{13}C NMR (50 MHz, $CDCl_3$): δ 174.8, 160.2, 157.5, 134.4, 129.1, 113.5, 70.0, 55.1, 38.7, 37.4, 34.7, 31.1, 27.4, 25.6, 24.6, 17.9, −5.1; MS (ESI) m/z (%): 451.8 [(M+H)[+], 100].

(*Z*)-2-(*tert*-Butyldimethylsilyloxy)-3-(4-methoxyphenethylthio)-*N'*-(pivaloyloxy)propanimidamide (39b)

Yield 73%; colorless oil; ^{1}H NMR (200 MHz, $CDCl_3$): δ 7.06 (2H, d, J = 8.6 Hz), 6.78 (2H, d, J = 8.6 Hz), 5.15–4.84 (2H, m), 4.55–4.43 (1H, m), 3.74 (3H, s), 2.89–2.70 (6H, m), 1.24 (9H, s), 0.88 (9H, s), 0.11 (3H, s), 0.07 (3H, s); ^{13}C NMR (50 MHz, $CDCl_3$): δ 174.6, 158.9, 157.8, 132.3, 129.2, 113.6, 69.7, 55.0, 38.7, 35.1, 34.7, 28.3, 27.3, 25.5, 17.9, −5.1, −5.3; MS (ESI) m/z (%): 469.3 [(M+H)[+], 100].

Synthesis of 40a,b

To a stirred solution of compound **39a,b** (1.0 mmol) in dry toluene (3 mL) in a microwave vessel, TBAF (1M in THF, 1.0 mmol) was added. The reaction mixture was left stirring under microwave irradiation (initial setting at 90W) for 1 hour at 120 °C. The organic solvent was evaporated under reduced pressure and the residue was purified by column chromatography [EtOAc-petroleum ether (bp 40–60 °C), 2:8].

1-(5-*tert*-Butyl-1,2,4-oxadiazol-3-yl)-5-(4-methoxyphenyl)pentan-1-ol (40a)

Yield 28%; colourless solid; m.p. 109- 111°C; ^{1}H NMR (200 MHz, $CDCl_3$): δ 7.09 (2H, d, J = 8.0 Hz), 6.81 (2H, d, J = 8.0 Hz), 4.82 (1H, t, J = 6.0 Hz), 3.78 (3H, s), 2.92 (1H, s), 2.57 (2H, t, J = 6.0 Hz), 2.02–1.87 (2H, m), 1.75–1.55 (4H, m), 1.43 (9H, s); ^{13}C NMR (50 MHz, $CDCl_3$): δ 186.4, 171.7, 157.5, 134.4, 129.1, 113.6, 66.6, 55.1, 35.3, 34.7, 33.0, 31.2, 28.3, 24.6; MS (ESI) m/z (%): 319.2 [(M+H)[+], 100].

1-(5-*tert*-Butyl-1,2,4-oxadiazol-3-yl)-2-(4-methoxyphenethylthio)ethanol (40b)

Yield 25%; pale yellow oil; ^{1}H NMR (200 MHz, $CDCl_3$): δ 7.11 (2H, d, J = 8.6 Hz), 6.84 (2H, d, J = 8.6 Hz), 5.04–4.86 (1H, m), 3.79 (3H, s), 3.31–3.18 (1H, m), 3.11–3.01 (2H, m), 2.91–2.69 (4H, m), 1.43 (9H, s); ^{13}C NMR (50 MHz, $CDCl_3$): δ 186.8, 170.3, 158.2, 132.0, 129.4, 113.9, 65.4, 55.2, 37.9, 35.2, 34.2, 33.7, 28.3; MS (ESI) m/z (%): 337.2 [(M+H)[+], 100].

Synthesis of 1,2,4-oxadiazoles 32, 33

To a stirred solution of compound **40a,b** (1 mmol) in dry CH_2Cl_2 (10 mL), Dess-Martin periodinane was added (1.2 mmol, 509 mg) and the mixture was stirred for 1 h at room temperature. The organic solvent was evaporated under reduce pressure and Et_2O (30 mL) was added. The organic phase was washed with saturated aqueous $NaHCO_3$ (20 mL) containing $Na_2S_2O_3$ (1.5 g, 9.5 mmol), H_2O (20 mL), dried over Na_2SO_4, and the organic solvent was evaporated under reduced pressure. The residue was purified by column chromatography [EtOAc-petroleum ether (bp 40–60 °C), 2:8].

1-(5-*tert*-Butyl-1,2,4-oxadiazol-3-yl)-5-(4-methoxyphenyl)pentan-1-one (33)

Yield 88%; colourless oil; ^{1}H NMR (200 MHz, $CDCl_3$): $\delta = 7.08$ (2H, d, $J = 8.0$ Hz), 6.81 (2H, d, $J = 8.0$ Hz), 3.77 (3H, s), 3.06 (2H, t, $J = 6.0$ Hz), 2.59 (2H, t, $J = 6.0$ Hz), 1.86–1.64 (4H, m), 1.47 (9H, s); ^{13}C NMR (50 MHz, $CDCl_3$): $\delta = 191.8$, 187.8, 165.3, 157.6, 134.0, 129.2, 113.6, 55.2, 40.3, 34.6, 33.8, 30.9, 28.3, 23.0; HRMS (ESI) calcd for $C_{18}H_{24}N_2O_3$ [M+H]$^+$, 317.1863, found, 317.1863.

1-(5-*tert*-Butyl-1,2,4-oxadiazol-3-yl)-2-(4-methoxyphenethylthio)ethanone (32)

Yield 85%; colorless oil; ^{1}H NMR (200 MHz, $CDCl_3$): δ 7.13 (2H, d, $J = 8.6$ Hz), 6.83 (2H, d, $J = 8.6$ Hz), 3.86–3.70 (5H, m), 2.94–2.70 (4H, m), 1.49 (9H, s); ^{13}C NMR (50 MHz, $CDCl_3$): δ 188.2, 184.4, 164.7, 158.2, 131.8, 129.5, 113.8, 55.2, 37.6, 34.4, 33.9, 33.8, 28.3; HRMS (ESI) calcd for $C_{17}H_{21}N_2NaO_3S$ [M+Na]$^+$, 357.1243, found, 357.1255.

Supplementary Material

Refer to Web version on PubMed Central for supplementary material.

Acknowledgments

Abbreviations used

PLA$_2$	Phospholipase A$_2$
cPLA$_2$	cytosolic
sPLA$_2$	secreted
iPLA$_2$	calcium-independent
PAF-AH	platelet-activating factor acetylhydrolase
Lp-PLA$_2$	lipoprotein-associated

LPLA$_2$	lysosomal
AdPLA	adipose-PLA
AA	arachidonic acid
GVIA cPLA$_2$	Group IVA cytosolic
GVIA iPLA$_2$	Group VIA calcium-independent
GV sPLA$_2$	Group V secreted
COX	cyclooxygenase
LOX	lipoxygenase
DXMS	hydrogen/deuterium exchange mass spectrometry
MD	molecular dynamics
SAR	structure-activity relationship
IFD	Induced Fit Docking
XP GScore	extra-precision glide score
X$_I$(50)	mole fraction of the compound that is required for 50% inhibition of the enzyme
TBDMSCN	*tert*-butyldimethylsilyl cyanide
DCC	*N,N'*-dicyclocarbodiimide
TBAF	tetrabutylammonium fluoride
PAPC	1-palmitoyl-2-arachidonoyl-*sn*-glycero-3-phosphocholine
CGenFF	CHARMM General Force Field
VMD	visual molecular dynamics

References

1. Dennis E, Cao J, Hsu YH, Magrioti V, Kokotos G. Phospholipase A$_2$ enzymes: physical structure, biological function, disease implication, chemical inhibition, and therapeutic intervention. Chem Rev. 2011; 111:6130–6185. [PubMed: 21910409]

2. Dennis EA, Norris PC. Eicosanoid storm in infection and inflammation. Nat Rev Immunol. 2015; 15:511–523. [PubMed: 26139350]

3. Mouchlis VD, Dennis EA. Membrane and inhibitor interactions of intracellular phospholipases A$_2$. Adv Biol Regul. 2015; doi: 10.1016/j.jbior.2015.11.011

4. Kramer RM, Roberts EF, Manetta J, Putnam JE. The Ca^{2+}-sensitive cytosolic phospholipase A$_2$ is a 100-kDa protein in human monoblast U937 cells. J Biol Chem. 1991; 266:5268–5272. [PubMed: 2002059]

5. Sharp JD, White DL, Chiou XG, Goodson T, Gamboa GC, McClure D, Burgett S, Hoskins J, Skatrud PL, Sportsman JR. Molecular cloning and expression of human Ca^{2+}-sensitive cytosolic phospholipase A$_2$. J Biol Chem. 1991; 266:14850–14853. [PubMed: 1869522]

6. Clark JD, Lin LL, Kriz RW, Ramesha CS, Sultzman LA, Lin AY, Milona N, Knopf JL. A novel arachidonic acid-selective cytosolic PLA_2 contains a Ca^{2+}-dependent translocation domain with homology to PKC and GAP. Cell. 1991; 65:1043–1051. [PubMed: 1904318]

7. Dessen A, Tang J, Schmidt H, Stahl M, Clark J, Seehra J, Somers W. Crystal structure of human cytosolic phospholipase A_2 reveals a novel topology and catalytic mechanism. Cell. 1999; 97:349–360. [PubMed: 10319815]

8. Buczynski M, Dumlao D, Dennis E. Thematic review series: proteomics. an integrated omics analysis of eicosanoid biology. J Lipid Res. 2009; 50:1015–1038. [PubMed: 19244215]

9. Ackermann EJ, Kempner ES, Dennis EA. Ca^{2+}-independent cytosolic phospholipase A_2 from macrophage-like P388D1 cells. Isolation and characterization. J Biol Chem. 1994; 269:9227–9233. [PubMed: 8132660]

10. Ackermann EJ, Conde-Frieboes K, Dennis EA. Inhibition of macrophage Ca^{2+}-independent phospholipase A_2 by bromoenol lactone and trifluoromethyl ketones. J Biol Chem. 1995; 270:445–450. [PubMed: 7814408]

11. Larsson PK, Claesson HE, Kennedy BP. Multiple splice variants of the human calcium-independent phospholipase A_2 and their effect on enzyme activity. J Biol Chem. 1998; 273:207–214. [PubMed: 9417066]

12. Larsson Forsell PK, Kennedy BP, Claesson HE. The human calcium-independent phospholipase A_2 gene multiple enzymes with distinct properties from a single gene. Eur J Biochem. 1999; 262:575–585. [PubMed: 10336645]

13. Ramanadham S, Ali T, Ashley JW, Bone RN, Hancock WD, Lei X. Calcium-independent phospholipases A_2 ($iPLA_2s$) and their roles in biological processes and diseases. J Lipid Res. 2015; 56:1643–1668. [PubMed: 26023050]

14. Ayilavarapu S, Kantarci A, Fredman G, Turkoglu O, Omori K, Liu H, Iwata T, Yagi M, Hasturk H, Van Dyke TE. Diabetes-induced oxidative stress is mediated by Ca^{2+}-independent phospholipase A_2 in neutrophils. J Immunol. 2010; 184:1507–1515. [PubMed: 20053941]

15. Malhotra A, Edelman-Novemsky I, Xu Y, Plesken H, Ma J, Schlame M, Ren MC. Role of calcium-independent phospholipase A_2 in the pathogenesis of Barth syndrome. PNAS. 2009; 106:2337–2341. [PubMed: 19164547]

16. Chen Y, Dennis EA. Expression and characterization of human group V phospholipase A_2. Biochim Biophys Acta. 1998; 1394:57–64. [PubMed: 9767110]

17. Shirai Y, Balsinde J, Dennis EA. Localization and functional interrelationships among cytosolic group IV, secreted group V, and Ca^{2+}-independent group VI phospholipase A_2s in P388D 1 macrophages using GFP/RFP constructs. Biochim Biophys Acta. 2005; 1735:119–129. [PubMed: 15967714]

18. Masuda S, Murakami M, Komiyama K, Ishihara M, Ishikawa Y, Ishii T, Kudo I. Various secretory phospholipase A_2 enzymes are expressed in rheumatoid arthritis and augment prostaglandin production in cultured synovial cells. FEBS J. 2005; 272:655–672. [PubMed: 15670148]

19. Magrioti V, Kokotos G. Phospholipase A_2 inhibitors for the treatment of inflammatory diseases: a patent review (2010 - present). Expert Opin Ther Pat. 2013; 23:333–344. [PubMed: 23294257]

20. Ong WY, Farooqui T, Kokotos G, Farooqui AA. Synthetic and natural inhibitors of phospholipases A_2: their importance for understanding and treatment of neurological disorders. ACS Chem Neurosci. 2015; 6:814–831. [PubMed: 25891385]

21. Six DA, Barbayianni E, Loukas V, Constantinou-Kokotou V, Hadjipavlou-Litina D, Stephens D, Wong AC, Magrioti V, Moutevelis-Minakakis P, Baker SF, Dennis EA, Kokotos G. Structure-activity relationship of 2-oxoamide inhibition of group IVA cytosolic phospholipase A_2 and group V secreted phospholipase A_2. J Med Chem. 2007; 50:4222–4235. [PubMed: 17672443]

22. Stephens D, Barbayianni E, Constantinou-Kokotou V, Peristeraki A, Six DA, Cooper J, Harkewicz R, Deems RA, Dennis EA, Kokotos G. Differential inhibition of group IVA and group VIA phospholipases A_2 by 2-oxoamides. J Med Chem. 2006; 49:2821–2828. [PubMed: 16640343]

23. Antonopoulou G, Barbayianni E, Magrioti V, Cotton N, Stephens D, Constantinou-Kokotou V, Dennis EA, Kokotos G. Structure-activity relationships of natural and non-natural amino acid-based amide and 2-oxoamide inhibitors of human phospholipase A_2 enzymes. Bioorg Med Chem. 2008; 16:10257–10269. [PubMed: 18993078]

24. Kokotos G, Hsu YH, Burke J, Baskakis C, Kokotos C, Magrioti V, Dennis E. Potent and selective fluoroketone inhibitors of group VIA calcium-independent phospholipase A_2. J Med Chem. 2010; 53:3602–3610. [PubMed: 20369880]

25. Magrioti V, Nikolaou A, Smyrniotou A, Shah I, Constantinou-Kokotou V, Dennis E, Kokotos G. New potent and selective polyfluoroalkyl ketone inhibitors of GVIA calcium-independent phospholipase A_2. Bioorg Med Chem. 2013; 21:5823–5829. [PubMed: 23916152]

26. Baskakis C, Magrioti V, Cotton N, Stephens D, Constantinou-Kokotou V, Dennis EA, Kokotos G. Synthesis of polyfluoro ketones for selective inhibition of human phospholipase A_2 enzymes. J Med Chem. 2008; 51:8027–8037. [PubMed: 19053783]

27. Yang H, Mosior M, Johnson C, Chen Y, Dennis E. Group-specific assays that distinguish between the four major types of mammalian phospholipase A_2. Anal Biochem. 1999; 269:278–288. [PubMed: 10221999]

28. Mouchlis VD, Bucher D, McCammon JA, Dennis EA. Membranes serve as allosteric activators of phospholipase A_2, enabling it to extract, bind, and hydrolyze phospholipid substrates. PNAS. 2015; 112:E516–E525. [PubMed: 25624474]

29. Bucher D, Hsu YH, Mouchlis VD, Dennis EA, McCammon JA. Insertion of the Ca^{2+}-independent phospholipase A_2 into a phospholipid bilayer via coarse-grained and atomistic molecular dynamics simulations. PLoS Comput Biol. 2013; 9:e1003156. [PubMed: 23935474]

30. Hsu YH, Bucher D, Cao J, Li S, Yang SW, Kokotos G, Woods V, McCammon J, Dennis E. Fluoroketone inhibition of Ca^{2+}-independent phospholipase A_2 through pinding pocket association defined by hydrogen/deuterium exchange and molecular dynamics. J Am Chem Soc. 2013; 135:1330–1337. [PubMed: 23256506]

31. Burke J, Babakhani A, Gorfe A, Kokotos G, Li S, Woods V, McCammon J, Dennis E. Location of inhibitors bound to group IVA phospholipase A_2 determined by molecular dynamics and deuterium exchange mass spectrometry. J Am Chem Soc. 2009; 131:8083–8091. [PubMed: 19459633]

32. Phillips J, Braun R, Wang W, Gumbart J, Tajkhorshid E, Villa E, Chipot C, Skeel R, Kalé L, Schulten K. Scalable molecular dynamics with NAMD. J Comput Chem. 2005; 26:1781–1802. [PubMed: 16222654]

33. Protein preparation wizard 2014–4; Epik version 2.4. Schrödinger, LLC; New York, NY: 2014. Impact version 5.9, Schrödinger, LLC, New York, NY, 2014; Prime version 3.2, Schrödinger, LLC, New York, NY, 2014. 2014

34. Snyder DW, Bach NJ, Dillard RD, Draheim SE, Carlson DG, Fox N, Roehm NW, Armstrong CT, Chang CH, Hartley LW. Pharmacology of LY315920/S-5920,[[3-(Aminooxoacetyl)-2-ethyl-1-(phenylmethyl)-1H-indol-4-yl] oxy] acetate, a Potent and Selective Secretory Phospholipase A_2 Inhibitor: A New Class of Anti-Inflammatory Drugs, SPI. J Pharmacol Exp Ther. 1999; 288:1117–1124. [PubMed: 10027849]

35. Carman G, Deems R, Dennis E. Lipid signaling enzymes and surface dilution kinetics. J Biol Chem. 1995; 270:18711–18714. [PubMed: 7642515]

36. Douglas BK, Hélène D, John RF, Jürgen B. Docking and scoring in virtual screening for drug discovery: methods and applications. Nat Rev Drug Discov. 2004; 3:935–949. [PubMed: 15520816]

37. Hammock BD, Abdel-Aal YAI, Mullin CA, Hanzlik TN, Roe RM. Substituted thiotrifluoropropanones as potent selective inhibitors of juvenile hormone esterase. Pestic Biochem Physiol. 1984; 22:209–223.

38. Ashour MBA, Hammock BD. Substituted trifluoroketones as potent, selective inhibitors of mammalian carboxylesterases. Biochem Pharmacol. 1987; 36:1869–1879. [PubMed: 3593399]

39. Holmeide AK, Skattebol L. Syntheses of some polyunsaturated trifluoromethyl ketones as potential phospholipase A_2 inhibitors. J Chem Soc, Perkin Trans 1. 2000:2271–2276.

40. Huwiler A, Feuerherm AJ, Sakem B, Pastukhov O, Filipenko I, Nguyen T, Johansen B. The ω3-polyunsaturated fatty acid derivatives AVX001 and AVX002 directly inhibit cytosolic phospholipase A_2 and suppress PGE_2 formation in mesangial cells. Br J Pharmacol. 2012; 167:1691–1701. [PubMed: 22831644]

41. Musmade DS, Pattan SR, Yalgatti MS. Oxadiazole a nucleus with versatile biological behaviour. IJPC. 2015; 5:11–20.

42. Maryanoff BE, Costanzo MJ. Inhibitors of proteases and amide hydrolases that employ an alpha-ketoheterocycle as a key enabling functionality. Bioorg Med Chem. 2008; 16:1562–1595. [PubMed: 18053726]

43. Beno BR, Yeung KS, Bartberger MD, Pennington LD, Meanwell NA. A survey of the role of noncovalent sulfur interactions in drug design. J Med Chem. 2015; 58:4383–4438. [PubMed: 25734370]

44. Induced fit docking protocol 2014. Vol. 2014. Schrödinger, LLC; New York, NY: 2014. Glide version 6.5, Prime version 3.8

45. Sherman W, Day T, Jacobson MP, Friesner RA, Farid R. Novel procedure for modeling ligand/receptor induced fit effects. J Med Chem. 2006; 49:534–553. [PubMed: 16420040]

46. Maestro, version 9.9. Vol. 2014. Schrödinger, LLC; New York, NY: 2014.

47. LigPrep, version 3.2. Vol. 2014. Schrödinger, LLC; New York, NY: 2014.

48. Glide, version 6.5. Vol. 2014. Schrödinger, LLC; New York, NY: 2014.

49. Prime, version 3.8. Vol. 2014. Schrödinger, LLC; New York, NY: 2014.

50. Friesner RA, Murphy RB, Repasky MP, Frye LL, Greenwood JR, Halgren TA, Sanschagrin PC, Mainz DT. Extra precision glide: docking and scoring incorporating a model of hydrophobic enclosure for protein-ligand complexes. J Med Chem. 2006; 49:6177–6196. [PubMed: 17034125]

51. Vanommeslaeghe K, Hatcher E, Acharya C, Kundu S, Zhong S, Shim J, Darian E, Guvench O, Lopes P, Vorobyov I, Mackerell AC. CHARMM general force field: A force field for drug-like molecules compatible with the CHARMM all-atom additive biological force fields. J Comput Chem. 2009; 31:671–690. [PubMed: 19575467]

52. Klauda JB, Venable RM, Freites JA, O'Connor JW, Tobias DJ, Mondragon-Ramirez C, Vorobyov I, MacKerell AD, Pastor RWC. Update of the CHARMM all-atom additive force field for lipids: validation on six lipid types. J Phys Chem B. 2010; 114:7830–7843. [PubMed: 20496934]

53. Humphrey W, Dalke A, Schulten K. VMD: visual molecular dynamics. J Mol Graph. 1996; 14:33–38. [PubMed: 8744570]
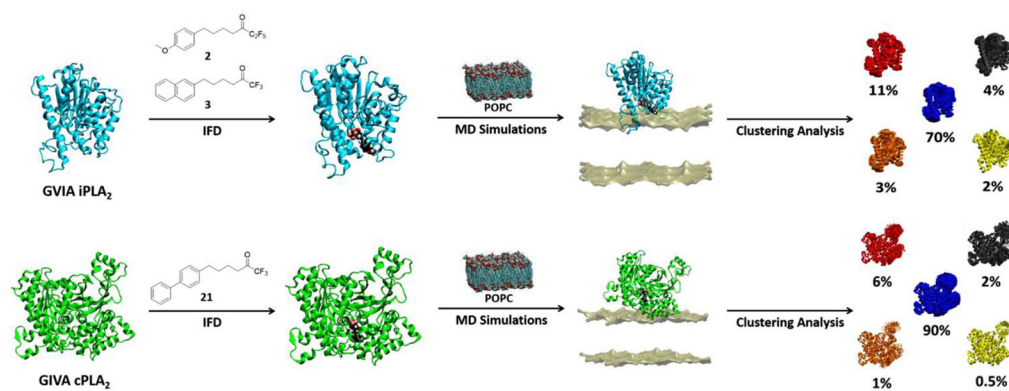
Figure 1. Structure-based design protocol
Fluoroketone inhibitors were docked in GVIA iPLA$_2$ and GIVA cPLA$_2$ binding site. Each enzyme-inhibitor complex was placed on a POPC membrane patch, solvated, minimized, equilibrated and subjected in 300 ns MD simulation. Suitable docking conformations of each complex were identifying using clustering analysis.
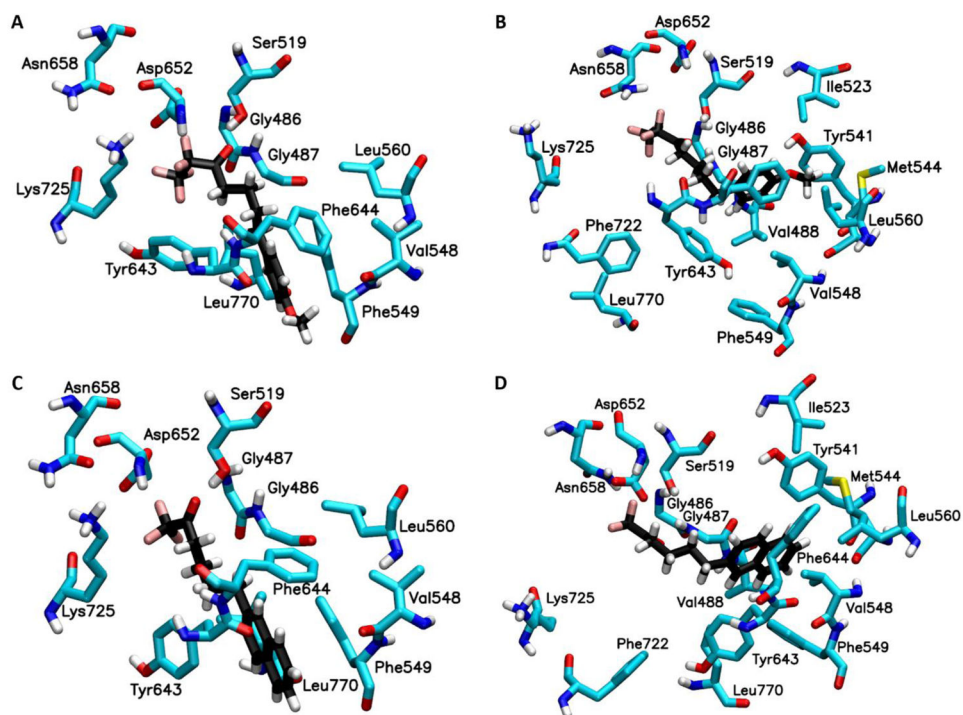
Figure 2. Binding mode of compound 2 and 3 in GVIA iPLA₂ binding pocket

(A) GVIA iPLA$_2$-**2** complex generated by IFD. (B) GVIA iPLA$_2$-**2** complex after MD simulation (Movie 1). (C) GVIA iPLA$_2$-**3** complex generated by IFD. (D) GVIA iPLA$_2$-**3** complex after MD simulation (Movie 2).
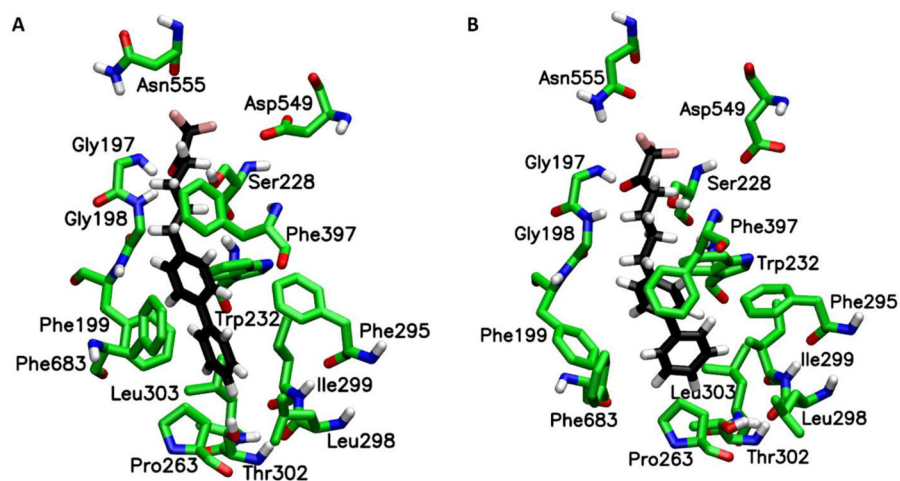
Figure 3. Binding mode of compound 21 in GIVA cPLA₂ binding pocket
(A) GIVA cPLA₂-**21** complex generated by IFD. (B) GIVA cPLA₂-**21** complex after MD simulation (Movie 3).
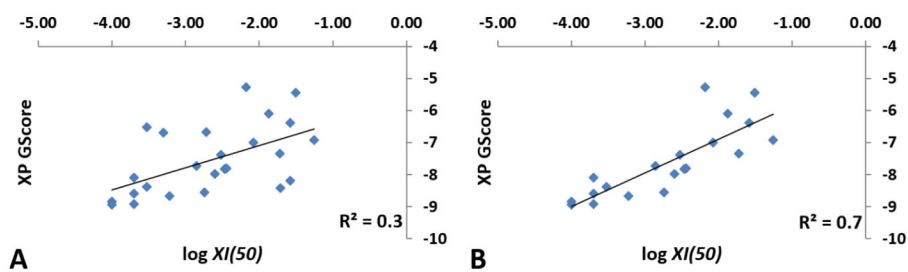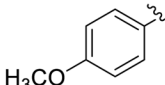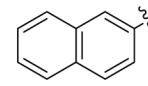
Figure 4. Correlation between the inhibitory activity (log X$_I$(50)) and the XP GScore
(A) All of the fluoroketone compounds were included. (B) Five outlier compounds were excluded (compounds **6**, **8**, **12**, **22** and **24** in Table 1).
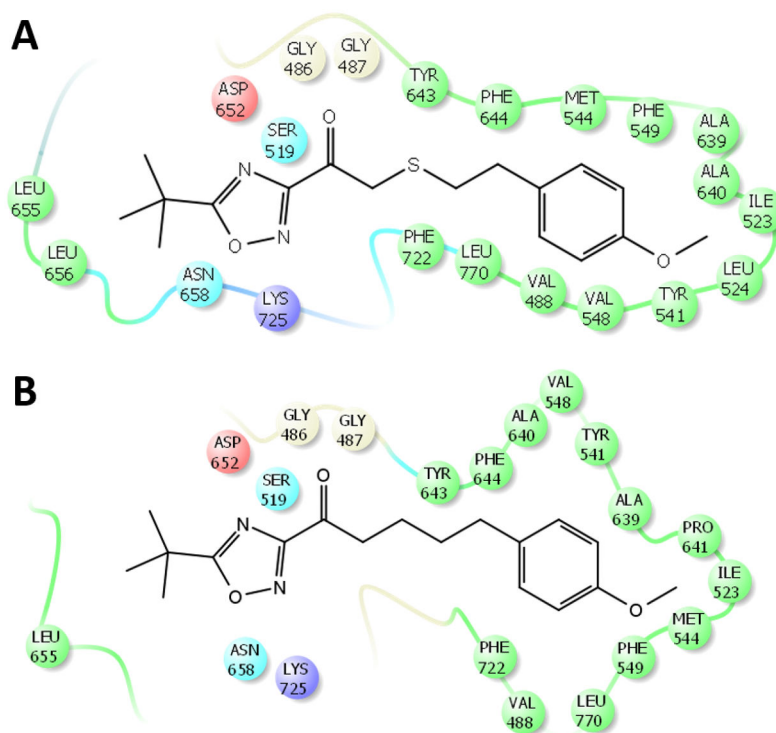
Figure 5.
Binding mode occur during the MD simulation for (A) compounds **32** (Movie 4) and for (B) compounds **33** (Movie 5) in GVIA iPLA$_2$ binding site.
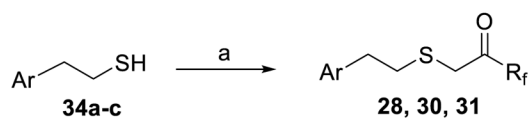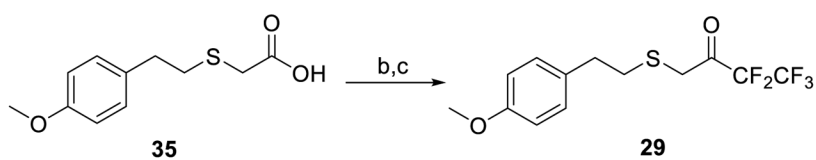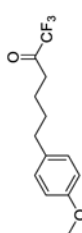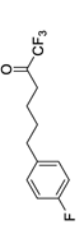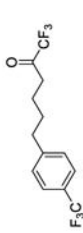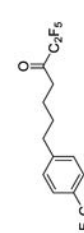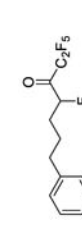
Scheme 1[a]

[a]Reagents and conditions: (a) $BrCH_2COCF_3$ or $BrCH_2COCF_2CF_3$, CCl_4; (b) N,O-dimethylhydroxylamine, DMAP, NMM, WSCI, CH_2Cl_2; (c) MeLi.LiBr, CF_3CF_2I, −78 °C.
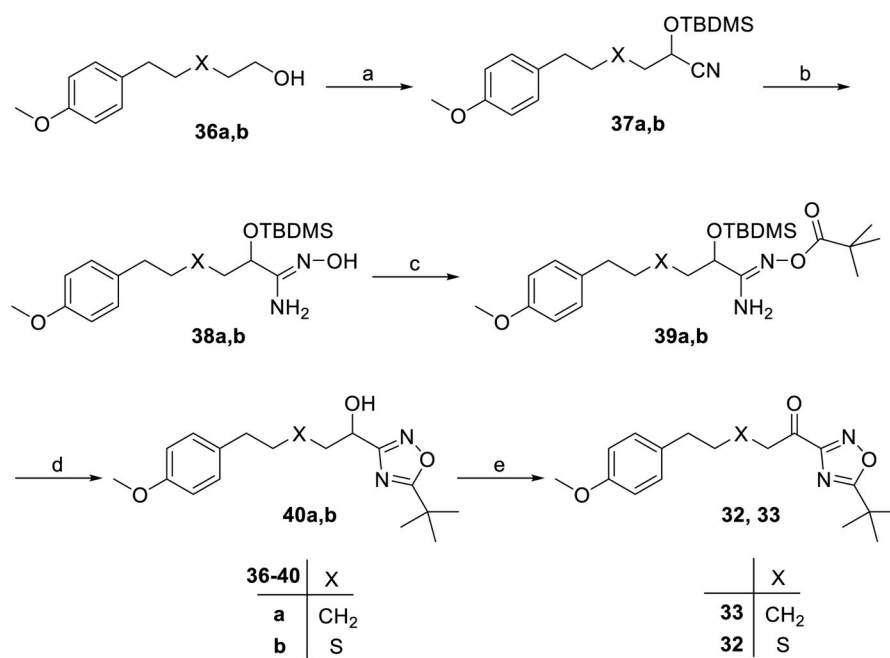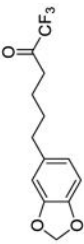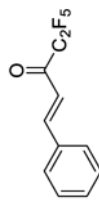
Scheme 2[a]
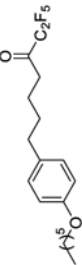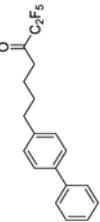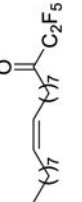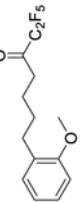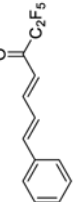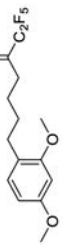
[a]Reagents and conditions: (a) i. Dess-Martin periodinane, CH_2Cl_2; ii. TBDMSCN, 18-crown-6, KCN, CH_2Cl_2; (b) 50% aq. NH_2OH, 50W; (c) pivalic acid, DCC, CH_2Cl_2; (d) TBAF, toluene, 90W; (e) Dess-Martin periodinane, CH_2Cl_2.

Table 1

Data set of fluoroketones used to generate SAR for GVIA iPLA$_2$

#	Structure	X$_I$(50)	log X$_I$(50)	XP GScore (GVIA iPLA$_2$)	XP GScore (GIVA cPLA$_2$)
1[a]		0.0001	−4.00	−8.9	−7.1
2[a]		0.0001	−4.00	−8.9	−6.7
3[b]		0.0002	−3.70	−8.9	−7.8
4[a]		0.0002	−3.70	−8.1	−6.9
5[a]		0.0002	−3.70	−8.6	−7.9
6[a]		0.0003	−3.52	−6.5	...
7[a]		0.0003	−3.52	−8.4	...
8[b]		0.0005	−3.30	−6.7	...
9[b]		0.0006	−3.22	−8.7	...

#	Structure	$X_I(50)$	log $X_I(50)$	XP GScore (GVIA iPLA$_2$)	XP GScore (GIVA cPLA$_2$)
10[b]		0.0014	−2.85	−7.7	−6.7
11[a]		0.0018	−2.74	−8.6	⋮
12[a]		0.0019	−2.72	−6.7	⋮
13[b]		0.0022	−2.66	ND*	⋮
14[a]		0.0025	−2.60	−8.00	⋮
15[b]		0.0030	−2.52	−7.4	⋮
16[a]		0.0034	−2.47	−7.8	⋮
17[b]		0.0036	−2.44	−7.8	⋮
18[b]		0.0066	−2.18	−5.3	⋮

#	Structure	$X_1(50)$	log $X_1(50)$	XP GScore (GVIA iPLA$_2$)	XP GScore (GIVA cPLA$_2$)
19[b]		0.0084	−2.08	−7.0	…
20[a]		0.0134	−1.87	−6.1	−9.8
21[a]		0.0189	−1.72	−7.3	−9.2
22[b]		0.0192	−1.72	−8.4	…
23[b]		0.0262	−1.58	−6.4	…
24[a]		0.0263	−1.58	−8.2	…
25[b]		0.0313	−1.50	−5.4	…
26[b]		0.0390	−1.41	ND*	…
27[a]		0.0553	−1.26	−6.9	…

Author Manuscript
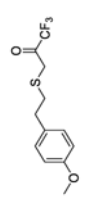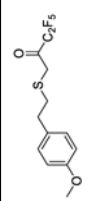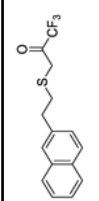
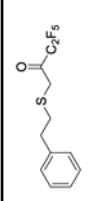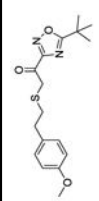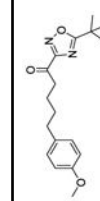[a]$X_I(50)$ value was reported elsewhere.[25]

[b]$X_I(50)$ value was reported elsewhere.[24]

*Glide could not produce a docking pose for these compound.

Author Manuscript

Author Manuscript

Author Manuscript

Table 2

XP GScore and $X_I(50)$ values for fluoroketone and keto-1,2,4-oxadiazole inhibitors

#	Structure	XP GScore (GVIA iPLA₂)	XP GScore (GIVA cPLA₂)	GVIA iPLA₂			GIVA cPLA₂	GV sPLA₂
				% Inh.	$X_I(50)$		% Inh.	% Inh.
28		−8.9	−6.8	96 ± 1	0.00009 ± 0.00001		60 ± 4	ND*
29		−8.9	−6.8	100 ± 1	0.00012 ± 0.00001		61 ± 4	28 ± 5
30		−8.8	−7.4	99 ± 1	0.0002 ± 0.00006		88 ± 1	32 ± 2
31		−8.4	−6.1	99 ± 1	0.00015 ± 0.00004		ND*	ND*
32		−7.4	−6.9	98 ± 0.4	0.0057 ± 0.0012		70 ± 2	38 ± 4
33		−4.3	−6.0	64 ± 4	…		52 ± 6	35 ± 6

*
Compound exhibited less than 25% or no detectable inhibition.